




Economical preparation of porous polyacrylonitrile-derived carbon/molybdenum disulfide composite anode for high-performance lithium-ion battery

Yixuan Huang¹, Jihua Zou¹, Lingzhi Luo¹, Zhixing Zhao², Hezhuang Liu¹, Yun Huang^{2,*}, Aobo Ren^{1,*} , and Zhiming Wang¹

¹Institute of Fundamental and Frontier Sciences, University of Electronic Science and Technology of China, Chengdu 610054, China

²School of New Energy and Materials, Southwest Petroleum University, Chengdu 610500, China

Received: 1 July 2021

Accepted: 12 October 2021

Published online:
3 January 2022

© The Author(s), under exclusive licence to Springer Science+Business Media, LLC, part of Springer Nature 2021

ABSTRACT

Two-dimensional (2D) materials combined with carbonaceous materials have shown remarkable properties for boosting the performance of lithium-ion batteries (LIBs). Precise spatial modulation and accurate transmission characteristics of electronic conductivity require good contact between materials. Herein, the preparation of a molybdenum disulfide/polyacrylonitrile-derived carbon (MoS₂/PDC) composite by heat treatment in argon atmosphere at 600 °C is presented. The polyacrylonitrile (PAN) and MoS₂ are subjected to phase inversion preparation membrane and lignin-assisted exfoliation pretreatment, respectively. The MoS₂ nanosheets can enter into the pore of PAN membrane and from C–S bonds during carbonization process, providing effective electron transport paths. Highly conductive carbonized PAN layer can act as an electron collector and provides the volume expansion space for MoS₂. Cell tests indicate that the MoS₂/PDC electrode exhibits an ultra-high lithium-ion storage capacity of 1354 mAh g⁻¹ at a current density of 0.1 A g⁻¹ and excellent cycling stability. With the advantages of low cost, green process and high electrochemical performance, the MoS₂/PDC composite is a promising anode material of LIBs.

Handling Editor: Mark Bissett.

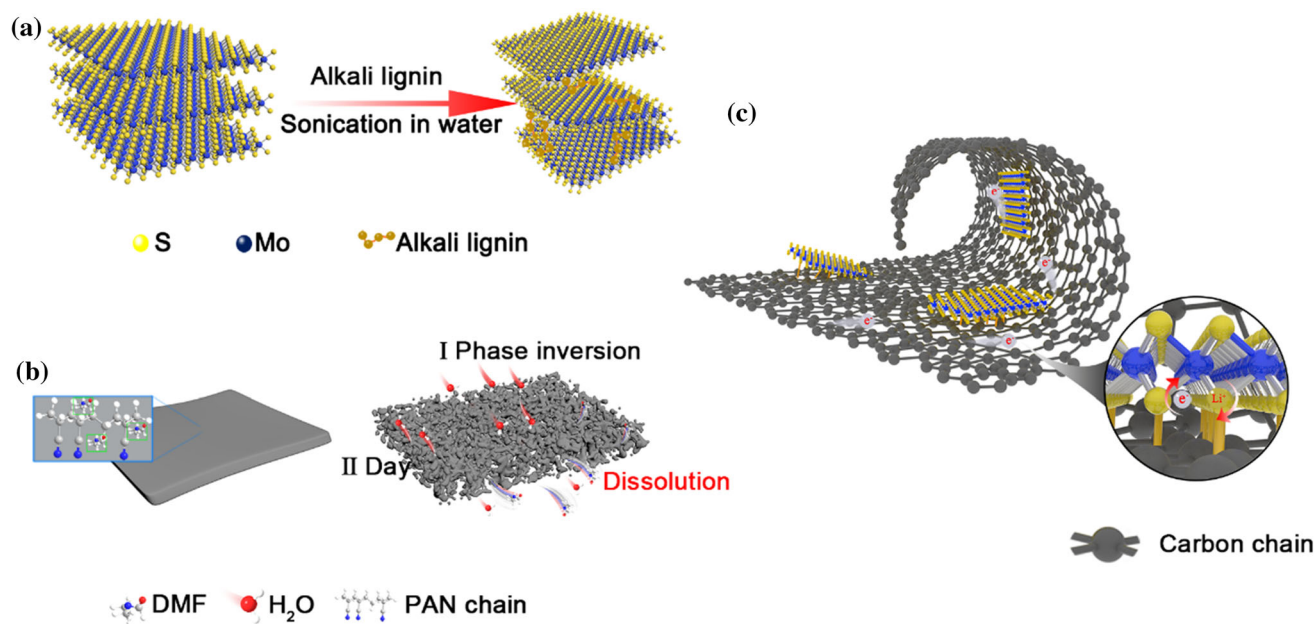
Address correspondence to E-mail: huangyun982@163.com; aobo.ren@uestc.edu.cn

Introduction

Since the discovery of graphene in 2014, two-dimensional (2D) materials have attracted numerous attention in energy storage field, particularly in lithium-ion batteries (LIBs) [1, 2]. Thanks to their unique chemical, electronic and mechanical properties, many efforts have been devoted to break the current limitations of anode materials [3–5]. Among various 2D materials, 2D-layered transition-metal dichalcogenides (TMDs) with thin atom layer have been extensively researched due to their high theoretical energy storage capacity and low fabrication cost [6, 7]. The currency conversion reaction between TMDs and Li: $MS_2 + Li^+ + e^- \rightarrow M + Li_2S$ ($M = Mo, W, \text{etc.}$) implies a complex electrochemical reaction process, which inspires the exploration of the chemical reaction processes [8]. Specifically, it has been demonstrated that monolayer molybdenum disulfide (MoS_2), one of the promising anode materials in LIBs, can be applied in low Li^+ migration barriers with high intrinsic conductivity [9, 10]. MoS_2 with short ion paths and highly exposed active sites also presents a significantly high initial capacity. In addition, the weak van der Waals interlayer in MoS_2 leads to a relatively large spacing between the adjacent layers with a higher energy storage capacity than the commercial graphite anode (670 mAh g^{-1} against 372 mAh g^{-1}) [11, 12]. Nevertheless, due to electrode structure collapse caused by volume expansion during cycling, the relatively low intrinsic conductivity and undesired cyclic stability strongly limit the rate capabilities of MoS_2 anodes [13–15]. Thanks to the larger surface area and more active edges of MoS_2 nanosheets, the electrochemical charge storage capacity is much larger than their bulk crystals [16, 17]. MoS_2 nanosheets can reduce the transfer distance of electron and ions, accelerating the exchange of electrons and ions in an electrode, thus reducing the polarization resistance of electrode [18, 19]. The instability of bulk crystals can be improved through non-crystallization of 2D materials. However, the low electrical conductivity still cannot be effectively implemented as electrodes. In this case, MoS_2 nanomaterials aggregate during the process of charging and discharging, resulting in the structural integrity and large irreversible capacity loss [13, 20, 21]. To solve such issues, several recent works have been reported to combine MoS_2 with

carbonaceous materials (e.g., graphene, carbon nanotubes (CNTs) and mesoporous carbon materials) for enhancing the conductivity and integrity of nanostructure [22–24]. Fang et al. [25] reported an in situ grown 2D mesoporous carbon/ MoS_2 heterostructures via supramolecular self-assembly of mono micelles under hydrothermal treatment, suggesting the capability of ultra-high lithium storage. Wang et al. [26] fabricated a 2D MoS_2 /graphene heterostructure through layered graphene-oxide-assisted ultrasonic exfoliate MoS_2 method, showing an ultra-high capacity of 1453 mAh g^{-1} at 0.1 A g^{-1} . Ren et al. [27] prepared a flexible 3D graphene@CNT@ MoS_2 hybrid foam anode, which exhibited a good conductivity and flexibility. However, due to the simply indexed as a point-to-point contact mode, most of the MoS_2 cannot sufficiently contact with carbon materials. In addition, Zhang et al. [28] developed a scalable method combining electrospinning and hydrothermal process to prepare MoS_2 -based composite fibers, which exhibited high capacity and cycling performance in a lithium battery. Yao et al. [29] prepared a 3D assembly of nitrogen-doped carbon nanofibers (NCFs) derived from PAN through combined electrospinning/carbonization technique. The high manufacturing cost and the relatively complex fabrication process of the involved carbonaceous materials are unfavorable in practical applications. In addition, the higher temperature of PAN-derived N-doped carbon produced is not conducive to the maintenance of disordered flexible segment carbon. Therefore, it is highly desired to design a low-cost and simple process to effectively improve the electrochemical performance of MoS_2 nanomaterial in LIBs.

Various exfoliation techniques have been applied for multilayer MoS_2 , including liquid-phase exfoliation, micromechanical exfoliation, direct chemical synthesis and chemical vapor deposition (CVD) [26, 30, 31]. The liquid-phase exfoliation method is favored to produce MoS_2 nanosheets in terms of economic and environmental concerns. To overcome the challenge caused by hydrophobicity of MoS_2 to liquid-phase exfoliation, surfactants are generally used to make the MoS_2 nanosheets in suspension. The exfoliation principle is shown in Scheme 1a. The surfactants with negatively charged rigid macromolecules can enter the interlayer of MoS_2 . Owing to the electrostatic repulsion and steric hindrance effect, the multilayer MoS_2 will be peeled into MoS_2



Scheme 1 (a) Exfoliation of schematic of bulk MoS₂; (b) schematic diagram of phase inversion; (c) schematic of C-S band in MoS₂/PDC composite.

nanosheets during the exfoliation process [32]. Recently, porous polymer membrane prepared by phase inversion plays an important role in electrolyte membrane of LIBs due to the merits of facile operation, low cost and high efficient [33, 34]. The principle of phase inversion is shown in Scheme 1b. After the polymer dissolves in the soluble solvent, it is immersed in the anti-solvent to replace the solvent, so that the solvent is separated from the polymer matrix [35]. The microspores formed are interconnected and highly porous and hence ensure more electrolyte absorption [36]. The lithium ions contained in the rich electrolyte can react quickly to accept electrons, which is capable to reduce the polarization of the electrode, thus improving the electrochemical performance of LIBs. Consequently, the formed microspores may provide a large basal for MoS₂. According to previous reports, PAN, a semi-crystalline organic polymer with nitrile (-C≡N) functional group attached to the polyethylene backbone as a unit structure, can be prepared as a porous polymer membrane [37]. Due to the electron-attracting induction effect of -C≡N, the highly active carbon atom of connecting -C≡N group and the edge S atom in MoS₂ forms a chemical bond in a high-temperature inert environment, providing an efficient electron transport channel and inhibiting polysulfide dissolution [38, 39]. More prominent, the volume

change of S can be coordinated with that of flexible segments of PAN polymer and effectively slow down the instability of MoS₂ [40]. Wang et al. [41] developed a polyacrylonitrile (PAN)-derived porous carbon by hybridizing with a small amount of MoS₂ nanosheets by ZnCl₂ through nitrile-zinc ion interactions. However, this is not conducive to the high activity of carbon atom of connecting -C≡N group because the negatively charged surface of MoS₂ nanosheets can absorb Zn²⁺, resulting in local enrichment of Zn²⁺. Tuning the interaction between carbonaceous materials and MoS₂ by adjusting space structure through physical action is the key to solve this problem.

In this work, the liquid-phase exfoliation method with water as the medium is used to prepare single- or few-layer MoS₂. The PAN polymer porous membrane is prepared by the phase inversion method as carbon-based substrate material for MoS₂ nanosheets. By controlling the size of the nanosheets and membrane, pore MoS₂ nanosheets are solid on the PAN-derived carbon during carbonization process through a direct coupling of edge sulfur atoms of MoS₂ with the carbon chain. Then, the MoS₂/PDC composite structure is shown in Scheme 1c. It is expected that the MoS₂ evenly distributed in the PAN membrane can fully expose the active sites and serve as an isolation layer to isolate the relock tendency of MoS₂,

which maximize the lithium storage of MoS₂ nanosheets. The formation of C–S bond ensures that electrons can be effectively transported to the active substances. The MoS₂-/PAN-derived carbon electrode exhibits high lithium-ion storage capacity of 1354 mAh g⁻¹ at the current density of 0.1 A g⁻¹ and excellent cycle performance of 540 mAh g⁻¹ and 461.9 mAh g⁻¹ at 0.1 A g⁻¹ and 1.0 A g⁻¹ after 100 cycles, respectively. Therefore, the pretreatment MoS₂-/PAN-derived carbon composite is expected to be a good candidate for high-performance LIBs' anode materials.

Materials and methods

Preparation of few-layered MoS₂

Firstly, 25 mg alkali lignin (AL) was dissolved in 100 ml deionized water to form a uniform aqueous solution. Then, 1.0 g bulk MoS₂ was added into the AL solution, and subsequently the mixture was continuously sonicated for 6 h under an ultrasound system. The obtained dispersion could stand for 3 days under natural conditions, forming a few-layered MoS₂ aggregated at the bottom of bottle and removing un-exfoliated MoS₂ on the surface of solution. The remaining dispersion was centrifuged for 15 min at 1500 rpm to further remove the un-exfoliated MoS₂, followed by suction filtration, repeated washing three times, and finally dried to obtain a relatively pure few-layered MoS₂ powder.

Preparation of MoS₂/PDC composite

The phase inversion method was used to prepare PAN membrane. The principle is shown in Scheme 1b. The PAN powder (200 mg) is first dissolved in N, N-dimethylformamide (DMF, 1.89 ml) with continuous stirring at 60 °C for 30 min until completely dissolved. Then, the solution was evenly poured onto a glass plate, which was slowly immersed into deionized water, and after more than ten seconds one kind of white membrane appeared on glass. The membrane was taken off and then dried in the electric blast oven at 60 °C for 6 h. To obtain the mass loss data of PAN membrane after carbonization, the PAN was carbonized separately at 600 °C for 2 h in argon. The mass loss data obtained is 45.5%. To obtain a carbon content of 10% in the final composite, the new PAN membrane and few-

layered MoS₂ were mixed at a ratio of 1: 4.8 by mass. A proper amount of deionized water was added, followed by ultrasonic for 30 min, so that MoS₂ can enter the pores of PAN membrane. At last, the mixture is heated to 200 °C and left for 30 min to remove deionized water and then was carbonized at 600 °C for 2 h in argon to obtain MoS₂/PDC composite (heating rate: 10 °C/min; argon flow rate: 80 ccm). The PAN-derived carbon is abbreviated as PDC. In this laboratory, three groups of control experiments will be carried out, which are bulk MoS₂, few-layered MoS₂ and bulk MoS₂/PDC composite.

Structural and morphological characterization

X-ray diffraction (XRD) of MoS₂ was emerged with an X-ray diffractometer DX-2700B at 40-kV generator voltage. Raman spectra were obtained using a confocal Raman spectrometer with an excitation wavelength at 633 nm. The structure characteristics of MoS₂/PDC composite were performed using XPS with a monochromatized AlK α X-ray source and FTIR in a wavenumber range of 4000–400 cm⁻¹. The morphology of the prepared PAN membrane and carbonized MoS₂/PDC composite was observed by scanning electron microscopy (SEM, ZEISS EV0 MA15). The thickness of few-layered MoS₂ is measured by atomic force microscope (AFM).

Electrochemical characterization

The electrochemical performances of MoS₂/PDC complex were evaluated by using a CR2032 cell with lithium metal as the counter and reference electrodes, a Celgard 2600 membrane as the separator, and LiPF₆ in EC/DMC/EMC (ethylene carbonate/dimethyl carbonate/ethyl methyl carbonate, 1/1/1, w/w/w, LBC305-01, battery grade) as the electrolyte. The preparation of anode round piece (diameter: 14 mm, mass loading of MoS₂: 2.0 mg cm⁻²) was carried out by mixing 85 wt% C/MoS₂ complex, 10 wt% carbon black, and 5 wt% polyvinylidene fluoride (PVDF). The internal dynamic characteristics of the cell were performed by cyclic voltammetry (CV) in the potential range of 0.01–3 V (vs. Li/Li⁺) and EIS method (CHI-660D electrochemical analyzer) between frequency 0.1–100,000 Hz. The charge–discharge performances were recorded using the Neware BTSe5V50mA battery test system between 0.01 and 3 V (vs. Li/Li⁺) at room temperature. The cycling

performance and Coulomb efficiency were measured at 0.1 A g^{-1} .

Results and discussion

Structural and morphological characterization

Figure 1a shows the X-ray diffraction (XRD) patterns of bulk MoS_2 and few-layered MoS_2 . All diffraction peaks of few-layered MoS_2 correspond to hexagonal 2H-MoS_2 without any other phases visible. The attenuation of the (002) reflection peak for the few-layered MoS_2 is compared to the bulk MoS_2 , which proves that MoS_2 was exfoliated successfully. The absence of no characteristic diffraction peaks suggests that the overall structure of MoS_2 has not been

destroyed by the AL-assisted ultrasonic process. The Raman spectra of bulk MoS_2 and few-layered MoS_2 are shown in Fig. 1b-c. The high energy A_{1g} at higher wavenumber mode and E_{2g}^1 active mode at lower wavenumbers are observed in all MoS_2 samples, which represent the interlayer vibration and in-plane bending. In Fig. 1c, the red shift of A_{1g} peaks from 409.1 to 407.5 cm^{-1} can be ascribed to the weakened interlayer van der Waals force after exfoliation with the reduction of the number of layers. Typically, the E_{2g}^1 mode at 384 cm^{-1} of few-layered MoS_2 should show a blue shift due to the long-range interlayer Coulomb interactions compared with bulk MoS_2 . In our case, no significant blue shift of E_{2g}^1 peak is observed. This is because that the AL or solvent can be adsorbed on the surface of MoS_2 , thereby affecting

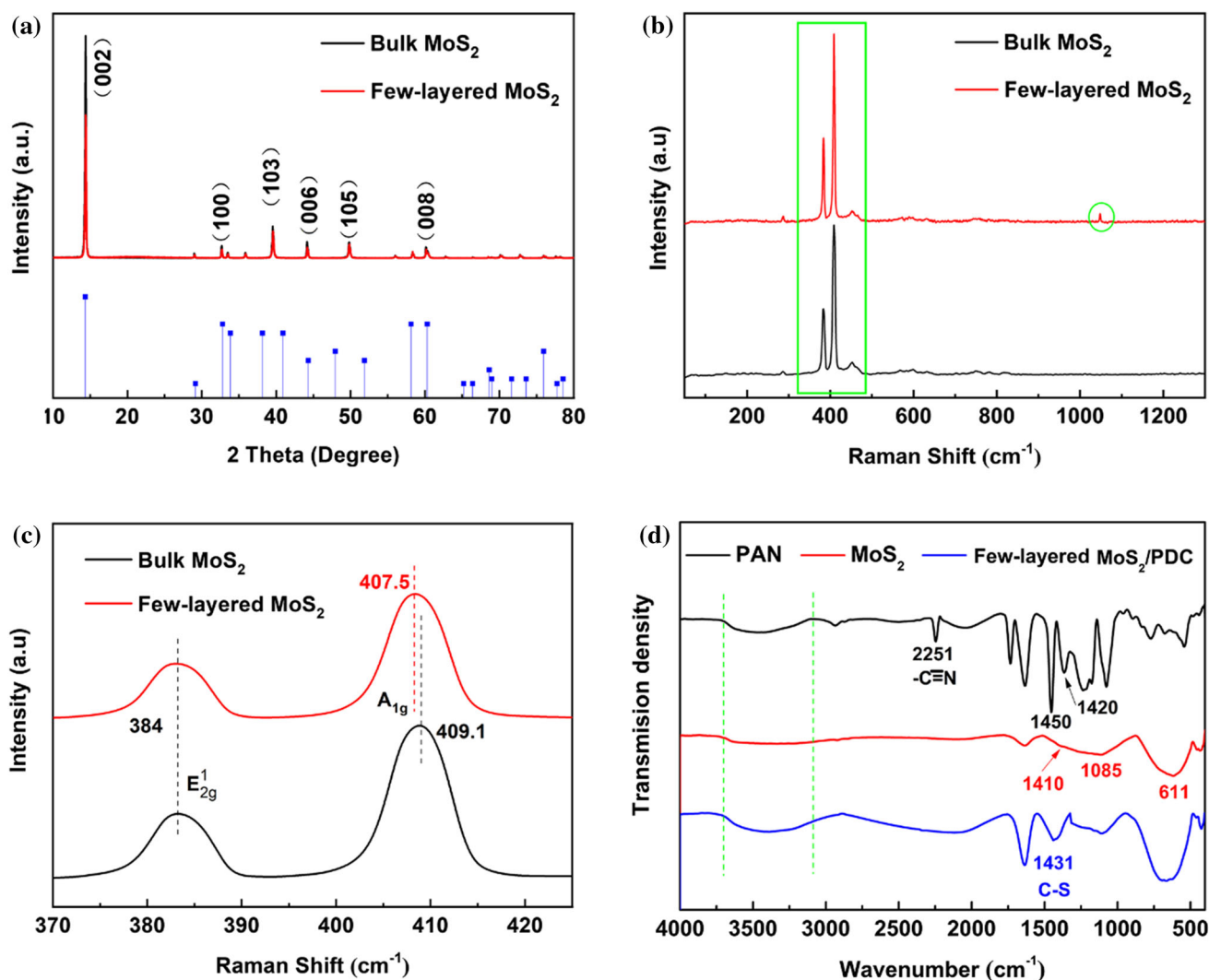


Figure 1 (a) XRD patterns of bulk MoS_2 and few-layered MoS_2 ; (b, c) Raman spectra of bulk MoS_2 and few-layered MoS_2 at 633 nm ; (d) FTIR spectrum of PAN polymers, MoS_2 and few-layered MoS_2/PDC composite.

in-plane atomic bending vibration. In addition, a peak at 1050 cm^{-1} of few-layered MoS_2 suggests the formation of defects on MoS_2 surfaces. As shown in Figure S1, the defects make S atoms have lone pairs of electrons, which is conducive to the formation of more C–S bonds.

We then investigate the structure of MoS_2 and PAN composite after carbonization. Figure 1d shows Fourier transform infrared (FTIR) spectra of PAN, few-layered MoS_2 and few-layered MoS_2/PDC composite. The peak at 2243 cm^{-1} represents the stretching vibration of nitrile group ($-\text{C}\equiv\text{N}$) as characteristic group in PAN. The characteristic peaks at 1450 cm^{-1} and 1420 cm^{-1} are corresponding to the vibration of $-\text{CH}_3$ and $-\text{CH}_2$, respectively, which are disappeared in the few-layered MoS_2/PDC composite after carbonization. Note that the broad bands between 3700 and 3200 cm^{-1} are attributed to the $-\text{OH}$ stretching of the free water in the air or residual water on the sample [42]. The absorptions at 1410 , 1085 and 611 cm^{-1} can be attributed to the MoS_2 [43]. The peak at 1431 cm^{-1} in the few-layered MoS_2/PDC composite is caused by the stretching vibration of the C–S bond. In Figure S2, the peak at 1421 cm^{-1} can also be expressed in the bulk MoS_2/PDC composite, confirming that the bulk MoS_2 and PAN can also form C–S bonds after carbonization. To clarify the interface properties between MoS_2 and carbon chain, the X-ray photoelectron spectroscopy (XPS) of few-layered MoS_2/PDC composite is carried out as shown in Fig. 2. Mo, S, C and O elements are observed in the MoS_2/PDC composite. It can be calculated from XPS spectra that the Mo/S atomic ratio is close to 1:2, which indicates that a stable MoS_2 structure exists in the MoS_2/PDC composite after carbonization. In detailed XPS spectra of S2p (Fig. 2b), two peaks at 163.5 and 162.4 eV represent S $2p_{1/2}$ and S $2p_{3/2}$ of S^{2-} , respectively. The detailed XPS spectra of Mo 3d core levels are shown in Fig. 2c. There are two peaks at 232.5 and 229 eV represented to Mo $3d_{3/2}$ and Mo $3d_{5/2}$ binding energies of Mo^{4+} , respectively. Meanwhile, the components centered at 235.5 eV can be ascribed to $3d_{3/2}$ of Mo^{6+} (typical of the Mo–O), which may be due to the reaction of MoS_2 with dilute oxygen at high temperature. The peak at 226.2 eV corresponds to the S 2s component. Figure 2d shows the high-resolution XPS spectrum of C 1s. Two peaks at 284.7 and 286.5 eV are assigned to C–C and C–O bands. The peaks at 289.4 eV can be ascribed to C = O bands, which indicates that the

part of the conjugated planes or pseudo-graphite microcrystal are formed during carbonization. It is noteworthy that a weak peak at 287.8 eV verifies the existence of C–S bonds, indicating that electron transfer occurs in the hybrid structure of the MoS_2/PDC sample. The model of C–S bond interactions is schematically demonstrated in Scheme 1c. As discussed above, the existence of C–S bonds between MoS_2 and carbon chain enhances the electron transport rate and structural stability.

The surface morphologies of PAN membrane, bulk MoS_2 , few-layered MoS_2 and few-layered MoS_2/PDC composite are shown in Fig. 3a–e. After phase inversion, it can be seen that the surface of PAN membrane shows an ordered pore network structure. A huge number of cavities are in large domains, and many interconnected pores have pore size ranging from 1.0 to 1.5 μm (Fig. 3a). The particle size of the MoS_2 powder is selected as 0.5–1.0 μm , ensuring that MoS_2 sheet can enter into the pores of PAN membrane. As shown in Fig. 3e, the atomic force microscope (AFM) image indicates that the few-layered MoS_2 sheet has a two- to five-layered structure with a thickness of 3.2 nm. TEM results for the exfoliated MoS_2 sonicated as shown in Fig. 3f, g indicate that the samples have a sheet structure in irregular shapes. Meanwhile, it reveals the periodic atomic arrangement of MoS_2 nanosheets at selected positions, and the measured interplanar spacing is 0.62 nm. Before carbonation, MoS_2 enters into the pores of PAN membrane due to fluid movement (Fig. 3c). Then, even though the shrinkage of carbon chain after carbonization leads to the decrease of pore size, the pore structure is still maintained (Fig. 3d), which is instrumental in composite adapt to the volume change of MoS_2 during charging–discharging for few-layered MoS_2/PDC electrode. Such composite displays a fine contact between MoS_2 and carbon chain. The structure of the composite is further verified by the energy-dispersive spectroscopy (EDS) mappings. Figure S3 shows a rough distribution of C, O, S and Mo in a specific area. The Mo/S atomic ratio of MoS_2 nanosheets is close to 1:2. Combined with XPS, it can be recommended that the S atoms of MoS_2 interact with the carbon layer during the carbonization, and MoS_2 can be uniformly embedded in the carbon matrix to form a hierarchical mixed structure with potential electronic conductivity.

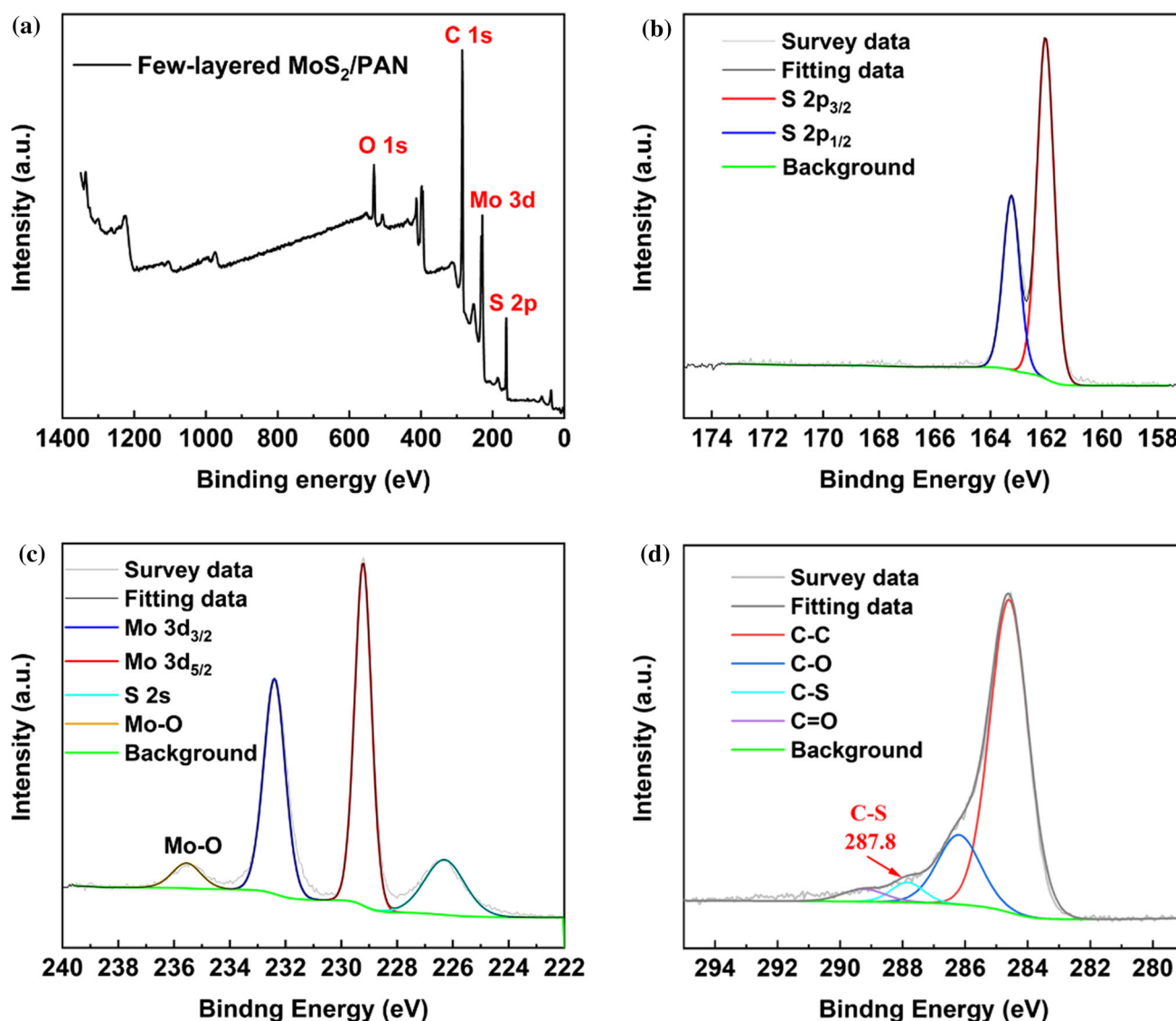


Figure 2 (a) XPS survey spectrum of few-layered MoS₂/PDC composite; (b–d) high-resolution spectra at three core levels: (b) S2p, (c) Mo3d, and (d) C1s.

Electrochemical performance

The electrochemical performances of MoS₂/PDC electrode are evaluated by using a CR2032 cell. Figure 4 shows the first three cyclic voltammetry (CV) curves of bulk MoS₂ and few-layered MoS₂/PDC electrode in a voltage range of 0.01–3.0 V at a scan rate of 1.0 mV s⁻¹. For the few-layered MoS₂/PDC electrode, there are two main reduction peaks at about 0.55 V and 0.25 V in the first cycle. The peak at 0.55 V is attributed to the insertion of Li⁺ into the MoS₂ layer, accompanied with a phase transition from 2H (triangular prism) to 1T (octahedron). The peak at 0.25 V is possibly caused by the further

insertion of Li⁺ into 1T-MoS₂, which may decompose and form Li₂S and Mo atoms. The anodic peak at 2.5 V is attributed to the oxidation of Li₂S to sulfur and Li⁺. In the following cycles, the two reduction peaks drift to 1.75 V and 1.0 V. The peak at 1.75 V is due to the reaction of S to S₈ and form a chain intermediate of Li₂S₈, accompanied with the dissolution reaction of Li₂S₈ to Li₂S_n ($n > 2$). The peak at 1.0 V is the transformation of soluble Li₂S_n to insoluble Li₂S or Li₂S₂. The peaks of Li₂S appeared in the XRD pattern after 3rd cycles in Figure S6, which further evidence that the lithium storage mechanism of MoS₂ is a conversion reaction. The process of producing different types of stored lithium is shown

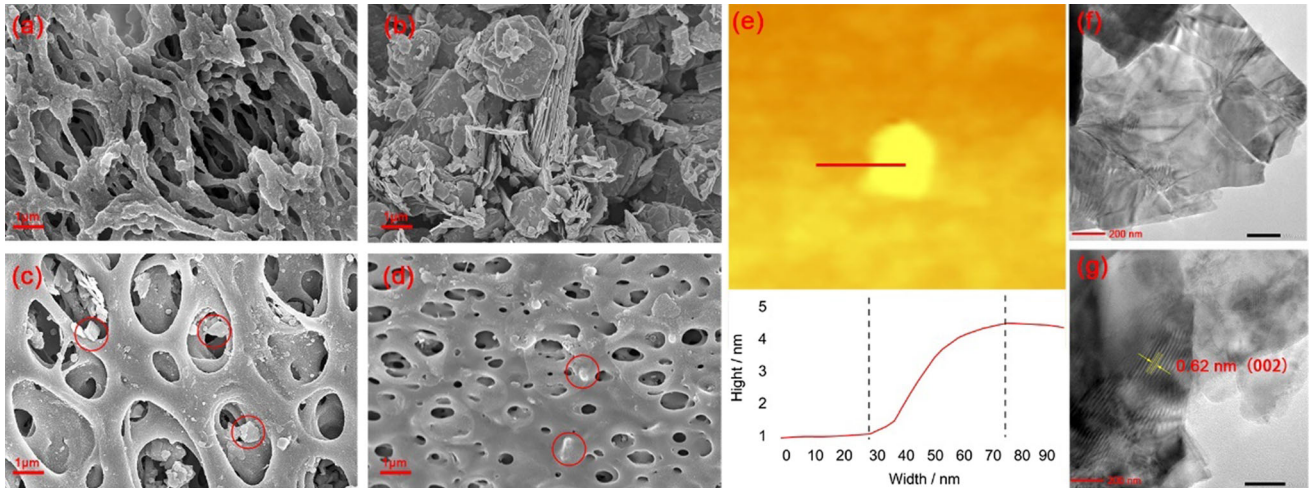


Figure 3 (a) SEM image of PAN membrane; (b) SEM image of bulk MoS₂; (c, d) SEM image of few-layered MoS₂/PDC composite before and after carbonization; (e) AFM image of

few-layered MoS₂ and surface height fluctuation curve; (f, g) TEM images of the exfoliated MoS₂ nanosheets.

in Fig. 4a. Interestingly, there is still a peak at 0.15 V, indicating that the transition from Li_xMoS₂ to Li₂S and Mo still exists. Therefore, the anodic peak at 1.0 V can be explained to a partial oxidation of Mo to form MoS₂, which can also be confirmed in Raman spectra in Figure S7. Both A_{1g} and E_{12g} exist in Figure S7 and only a relative red shift occurs, which is the result of partial collapse of MoS₂ structure. All the peaks are stable and appear in the third cycles, confirming the reversible electrochemical reaction process of MoS₂. It can be noticed that the S, Mo and MoS₂ are the main components of electrode material after the first cycle, instead of the initial MoS₂. This indicates that the active substance of storage lithium must be based on S apart from the first discharge, which can be easily dissolved in electrolyte, resulting in huge capacity loss [44, 45]. The formation of C–S bond in the MoS₂/PDC composite can just alleviate the phenomenon. As we expected, the peak of few-layered MoS₂/PDC electrode remains more stable compared to the bulk MoS₂ electrode in the following second three cycles (Figure S5), demonstrating an excellent stability. Compare to few-layered MoS₂/PDC electrode, the (002) diffraction peak of XRD pattern in Figure S6 is almost covered up for bulk MoS₂, explains the collapse of the overall structure. In addition, the potential gap between anodic and the first cathodic peaks for the few-layered MoS₂/PDC electrode (1.2 V) is smaller than that of multilayered MoS₂ electrode (1.3 V), indicating a smaller polarization for the few-layered MoS₂/PDC

electrode. Similar phenomenon occurred in other samples (Fig. 4c and Figure S4a–b). Moreover, the potential gap of multilayered MoS₂/PDC electrode and few-layered MoS₂ is less than 1.3 V, which suggests that the MoS₂ nanosheets and the formation of C–S bonds both can accelerate the exchange of electrons and ions, thus improving the battery performance.

To further explore the mechanism of energy storage for LIBs based on MoS₂/PDC electrode, the positions of reduction and oxidation peak are measured at different scanning rates from 0.2 to 5 mV s⁻¹ in Fig. 5a. With the increase in scanning rate, the current density of electrode increases, which is caused by the faster electron migration rate. Meanwhile, due to the mismatch of the acceleration rate between electron and ion, the potential gaps between anodic and cathodic peaks are broadened, leading to the incensement of polarization. The potentials of all few-layered MoS₂/PDC electrode are lower than those of bulk MoS₂ electrodes, implying that a batter rate matching of ions is presented. In Fig. 5c, d, the relationship between the peak current and the scanning rate can be expressed as a linear relationship between log*i* and log*v*, which proves that the diffusion process plays a major role in electrode and can be described by:

$$\log i = b \log v + \log a \tag{1}$$

where *i* is the peak current, *v* is the scan rate, *a* and *b* are the fitted constants and the *b* value can exactly

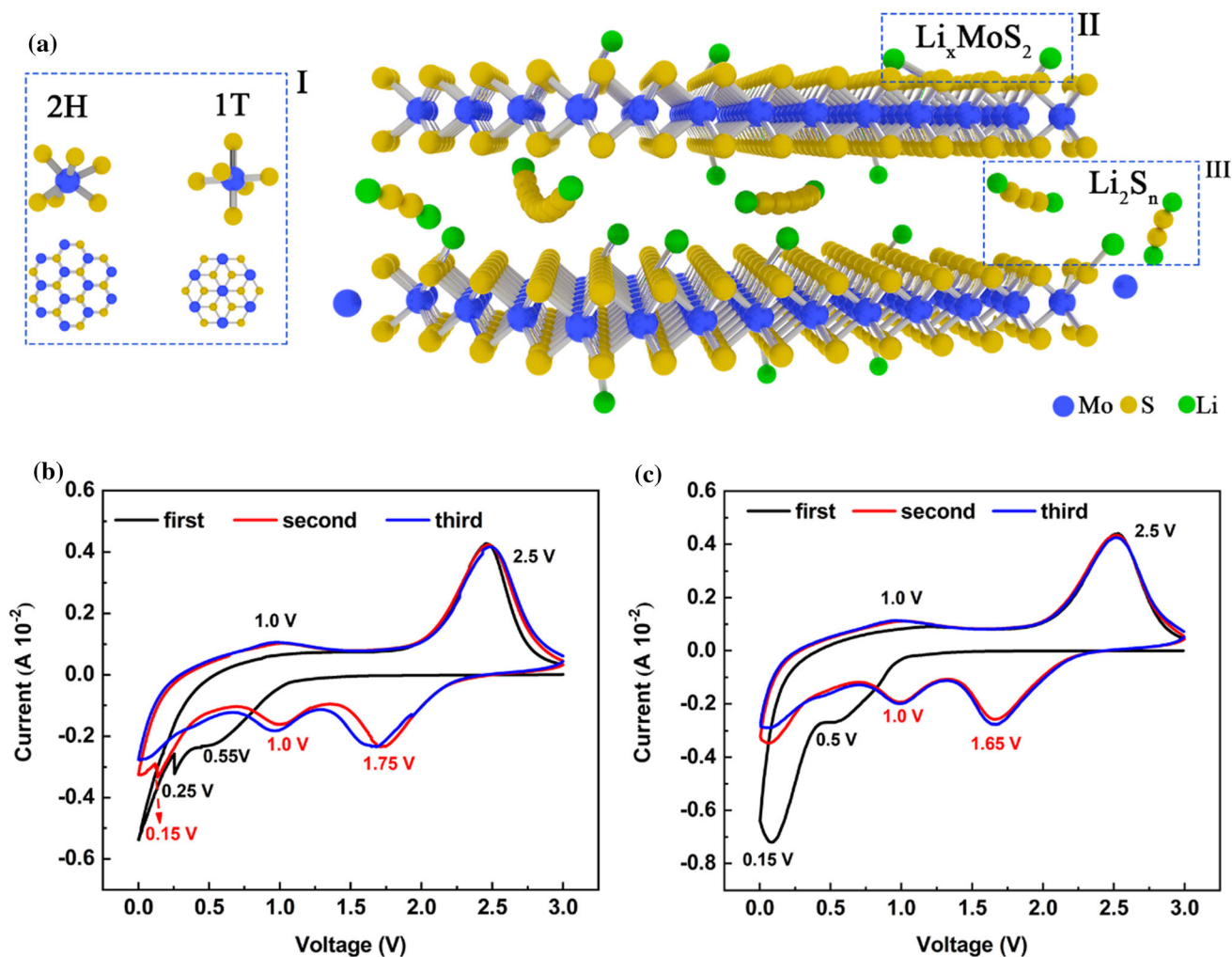


Figure 4 The schematic diagram of different types of storage lithium and conversion reaction (a); the first three cyclic voltammetry curves of the (b) few-layered MoS₂/PDC and (c) bulk MoS₂ electrode at a scanning rate of 1 mV s⁻¹.

reflect types of energy storage. The electrochemical energy storage can be divided into two types: Faraday intercalation and capacitance process. The system is mainly controlled by lithium-ion insertion process when the b value is near to 0.5, while the capacitance turns to dominant as the b value approaches to 1. The b values corresponding to all peaks are shown in Table 1. Although the b values of all peaks are close to 0.5 in both samples, the few-layered MoS₂/PDC electrode exhibits more efficient diffusion and electrochemical performance.

The electrochemical impedance spectra of all samples are shown in Fig. 6. In the Nyquist plots, the small semicircle at high frequency is the charge transfer resistance (R_{ct}), which can be attributed to the reaction of $\text{Li}^+ + \text{e}^- \leftrightarrow \text{Li}$ on the lithium metal electrode. The straight line at low frequency denotes

the open Warburg impedance (Z_w), whose slope has a positive correlation with the electrode diffusion coefficient [46, 47]. The intercepts at real axis under the high frequency remain unchanged for all samples, which are corresponding to the bulk resistance (R_b). The few-layered MoS₂/PDC electrode exhibits a minimum R_{ct} compared with the other three samples, indicating faster kinetics in the few-layered MoS₂/PDC electrode. It can be attributed to that MoS₂ nanosheets provide fast electron and ion migration channels and C–S bonds enhancing the transfer of the electron and Li⁺ [48]. The close binding of MoS₂ and PAN carbon chain enhances the electronic conductivity and the diffusion rate of Li⁺, which is beneficial to reduce electrode polarization. Meanwhile, the diffusion coefficient from the plots in the low-frequency region shows a maximum for few-layered

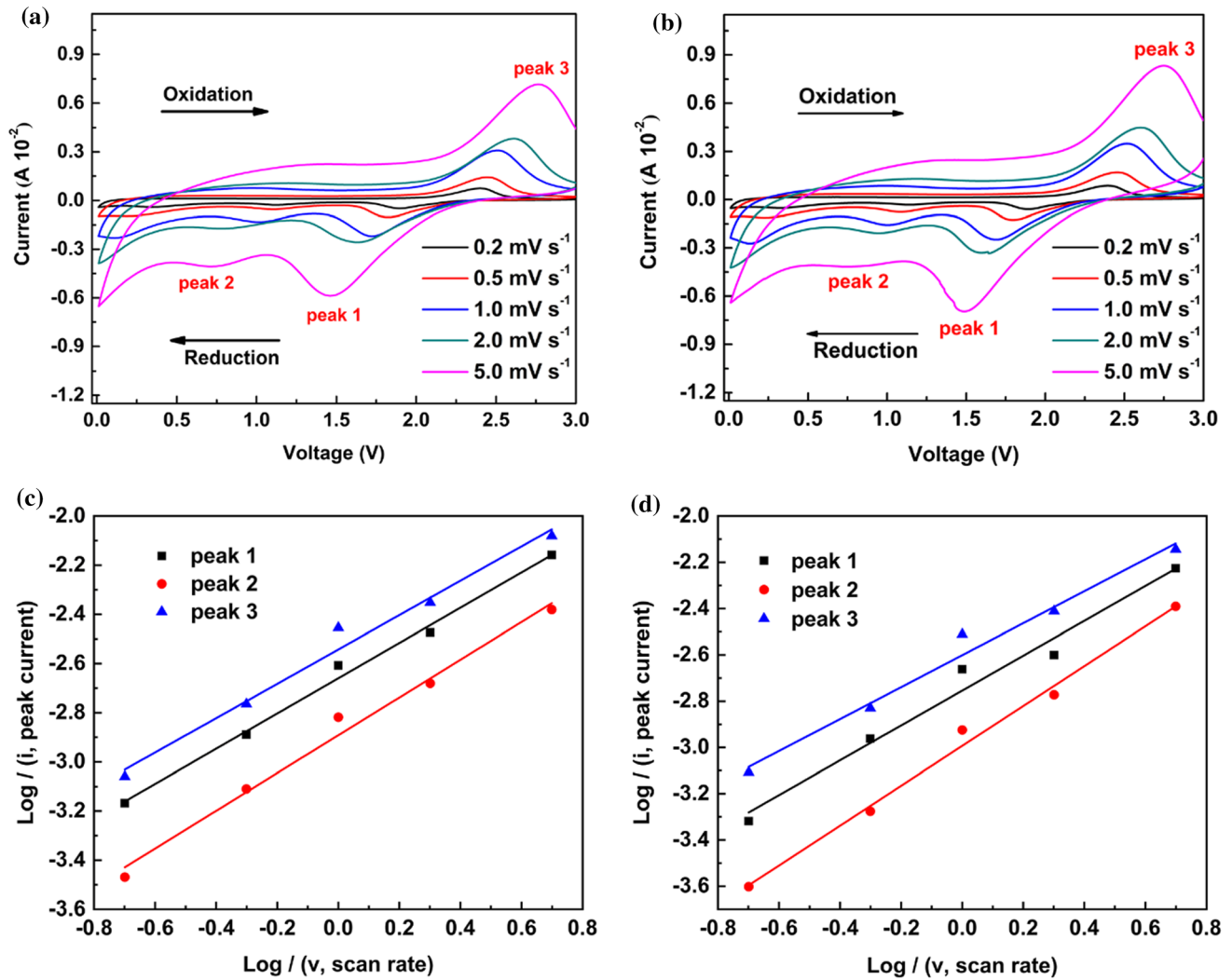


Figure 5 (a, b) Cyclic voltammograms of few-layered MoS₂/PDC electrode and bulk MoS₂ electrode at different scanning rates; (c, d) fitting curve of log(*i*) versus log(*v*).

Table 1 Slope value of log(*i*)–log(*v*) fitting curve

Peak	Bulk MoS ₂ <i>b</i> value	Few-layered MoS ₂ /PDC <i>b</i> value
1	0.75	0.72
2	0.86	0.77
3	0.69	0.69

MoS₂/PDC electrode, indicating that the PAN carbon chain can activate the microstructure of MoS₂ nanosheets. The reason is that the pore structure ensures the lithium ions contained in the rich electrolyte can react quickly to accept electrons. Moreover, the carbon chain provides a direct path for rapid lithium-ion diffusion, thus reducing the charge transfer resistance and increasing the diffusion of

ions. The most critical reason is that the existence of C–S bond in composite can increase the electronic and ionic conductivities, thus allowing fast transport of electrons and ions.

The charge/discharge performance is the most significant indicator for evaluating LIBs [49]. Figure 7a displays the typical charge/discharge curve of few-layered MoS₂/PDC electrode at the 1st, 5th, 10th, 50th and 100th cycles under a current density of 0.1 A g⁻¹ with a potential window of 0.01 V to 3.0 V (vs. Li/Li⁺). Firstly, the initial discharge capacity and charge capacity were 1321 mAh g⁻¹ and 1001 mAh g⁻¹, respectively. The capacity loss during the first cycle was possibly related to the formation of a solid electrolyte interface (SEI) on the electrode surface due to the decomposition of electrolyte [50]. In addition,

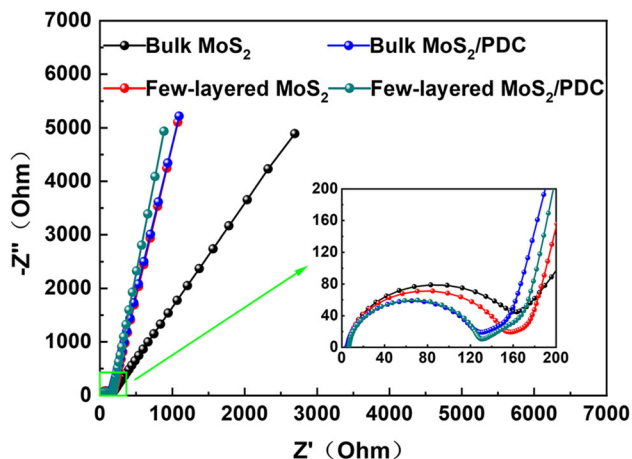


Figure 6 EIS curves of bulk MoS₂, few-layered MoS₂, bulk MoS₂/PDC and few-layered MoS₂/PDC between frequencies 0.1–100,000 Hz.

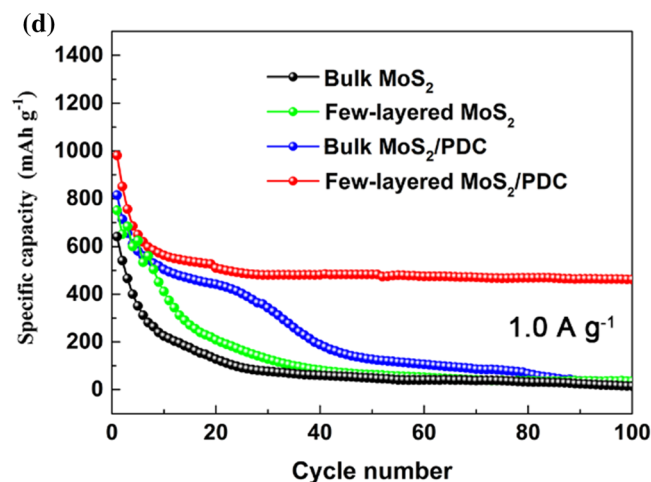
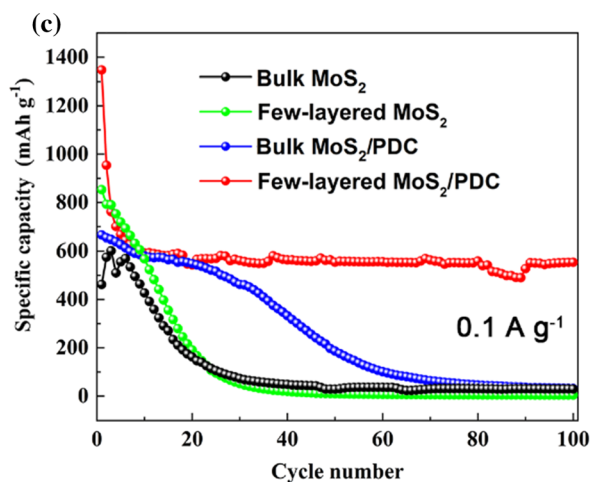
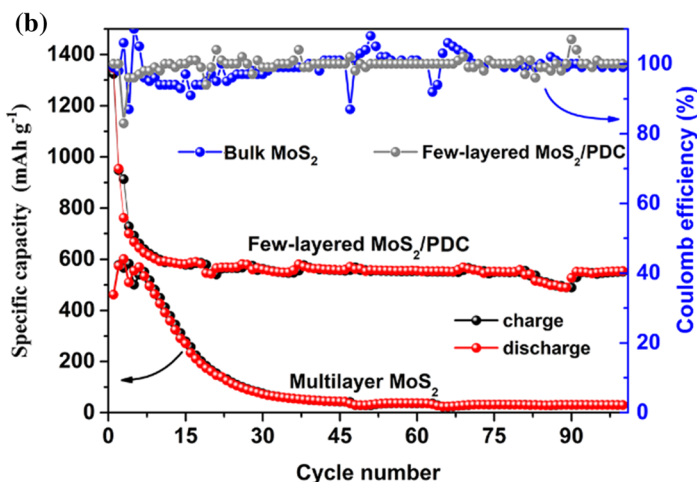
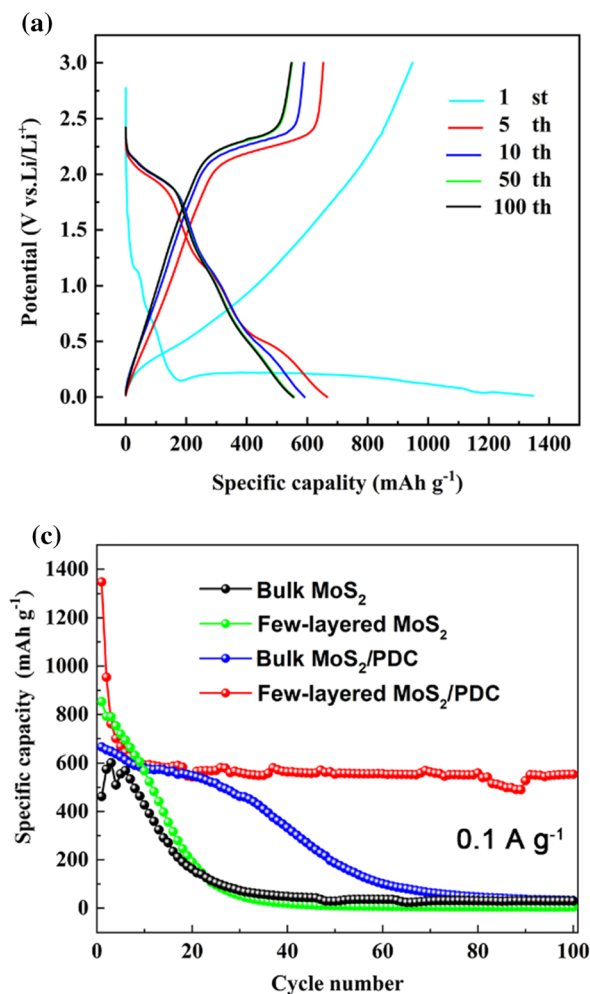


Figure 7 (a) The charge/discharge curves of few-layered MoS₂/PDC electrode between 0.01 and 3.0 V at a current density of 0.1 A g⁻¹; (b) Coulombic efficiency and cycling stability of few-

the uneven deposition of lithium on the surface of anode may hinder the insertion and dis-insertion of lithium. It is worth mentioning that the reversibility of capacity increases significantly in the 2nd and 3rd cycles, reaching 97% and 98%, respectively. On the contrary, the Coulomb efficiency of bulk MoS₂ cannot increase rapidly to 95% after three cycles, as shown in Fig. 7b. This can be attributed to that the flexible carbon segment in few-layered MoS₂/PDC composite ensures smooth electrochemical conversion of polysulfide and rapid lithium-ion migration. The result promotes the formation of an effective stable passivation layer and ensures the efficient reversible lithium-ion de-intercalate/intercalate process. Different discharge platforms between 0.1 and 2.25 V can be clearly seen in the 5th, 10th, 50th cycles, and

layered MoS₂/PDC electrode and bulk MoS₂; (c, d) cycling performance of bulk MoS₂, few-layered MoS₂, bulk MoS₂/PDC and few-layered MoS₂/PDC electrodes at 0.1 A g⁻¹ and 1.0 A g⁻¹.

the corresponding voltage can correspond to the characteristic peak of CV curve. There is no obvious capacity loss between 50 and 100th cycles, and the discharge capacity possess 540 mAh g^{-1} after 100th cycles, which is superior to the bulk MoS_2 (25 mAh g^{-1} after 100th cycles). The few-layered MoS_2/PDC electrode displays a higher specific capacity and excellent cycle stability compared to bulk MoS_2 from 5 to 100th cycles at 0.1 A g^{-1} (Fig. 7c). Next, the cell with few-layered MoS_2/PDC electrode can present a stable capacity of 461.9 mAh g^{-1} after 100 cycles at 1.0 A g^{-1} (Fig. 7d). Worse still, the MoS_2 electrode shows a specific capacity of only 14.8 mAh g^{-1} . Figure S8 shows the SEM image of lithium electrode after 100 cycles at 0.1 A g^{-1} for bulk MoS_2 (a) and few-layered MoS_2/PDC electrodes (b). For bulk MoS_2 , there are many bumpy particles on the surface of lithium anode, which are caused by the growth of lithium dendrite and the deposition of polysulfide, which lead the large fluctuations in the Coulomb efficiency of bulk MoS_2 . On the contrary, there are only a small number of particles and relatively smooth on the surface of lithium for few-layered MoS_2/PDC electrodes, indicating that excessive MoS_2 nanosheet can be prevented from dissolving and uneven deposition. The same phenomenon also appears on the bulk MoS_2 and few-layered MoS_2/PDC electrodes in Figure S9. The excellent performance can be ascribed to the following three reasons: First, the optimized electrolyte uptake of electrode ensures easier ion transmission and better retention of electrolyte during cycle. Second, the presence of C–S bonds can prevent excessive MoS_2 nanosheets deposition and facilitate electron and ion transport, thereby maintaining the cycling stability. Third, the carbon chain may be a more positive factor to improve the electrochemical performance. However, the bulk MoS_2/PDC electrode cannot exhibit the same outgoing properties (after 100th cycle at 0.1 A g^{-1} and 1.0 A g^{-1} , the discharge capacities are 35.2 mAh g^{-1} and 25.6 mAh g^{-1} , respectively) as few-layered MoS_2/PDC electrode. This may be attributed to the severe collapse caused by volume change of bulk MoS_2 , which inevitably reduces the interlayer structure and transmission path of ion. It is necessary to mention that all samples act out a similar large margin reversible capacity between 1st to 100th cycles, which are mainly attributed to the dissolution of polysulfide in the electrolyte and the insoluble product of reaction with electrolyte decomposition and electrode.

Conclusion

The composite of MoS_2 nanosheets and PAN polymer were successfully prepared by carbonization. Based on the clear porous structure of PAN membrane, the MoS_2 nanosheets, prepared by lignin-assisted exfoliation, can enter into the pore to form C–S bonds with PAN polymer during carbonization process, which facilitate electron transport and effectively inhibit polysulfide dissolution. Remarkably, the composite as an anode for LIBs exhibited outstanding specific capacities and excellent cycle performance. The fabricated porous structure can adapt to the volume change of sulfur and effectively slow down the instability of MoS_2 during the charge/discharge process. The few-layered MoS_2/PDC electrode exhibits an ultra-high discharge of 1354 mAh g^{-1} at 0.1 A g^{-1} and maintains 540 mAh g^{-1} and 461.9 mAh g^{-1} at 0.1 A g^{-1} and 1.0 A g^{-1} after 100 cycles, respectively. Moreover, the exposed active edges of MoS_2 nanosheets increase the extraction/insertion kinetics of Li^+ . This work provides a low-cost and simple process for preparing hybrid carbonaceous 2D materials for the LIBs with high energy storage capacity and stability.

Acknowledgements

This work was supported by the Fundamental Research Funds for the Central Universities (ZYGX2019Z018), the Innovation Group Project of Sichuan Province (20CXTD0090), and the “111 Project” (B20030).

Declarations

Conflicts of interest There are no conflicts to declare.

Supplementary Information: The online version contains supplementary material available at <http://doi.org/10.1007/s10853-021-06619-1>.

References

- [1] Mas-Ballesté R, Gómez-Navarro C, Gómez-Herrero J, Zamora F (2011) 2D materials: to graphene and beyond. *Nanoscale* 3:20–30. <https://doi.org/10.1039/c0nr00323a>

- [2] Ramakrishnan K, Nithya C, Karvembu R (2019) Heterostructure of two different 2D materials based on MoS₂ nanoflowers@rGO: an electrode material for sodium-ion capacitors. *Nanoscale Adv* 1:334–341. <https://doi.org/10.1039/C8NA00104A>
- [3] Long M, Wang P, Fang H, Hu W (2019) Progress, challenges, and opportunities for 2D material based photodetectors. *Adv Funct Mater* 29:1–28. <https://doi.org/10.1002/adfm.201803807>
- [4] Pomerantseva E, Gogotsi Y (2017) Two-dimensional heterostructures for energy storage. *Nat Energy*. <https://doi.org/10.1038/nenergy.2017.89>
- [5] Wen B, Guo R, Liu X et al (2020) Niobium oxyphosphate nanosheet assembled two-dimensional anode material for enhanced lithium storage. *J Energy Chem* 53:268–275. <https://doi.org/10.1016/j.jechem.2020.05.004>
- [6] Tabassum H, Zou R, Mahmood A et al (2018) A universal strategy for hollow metal oxide nanoparticles encapsulated into B/N co-doped graphitic nanotubes as high-performance lithium-ion battery anodes. *Adv Mater* 30:1–7. <https://doi.org/10.1002/adma.201705441>
- [7] Zhan C, Liu W, Hu M et al (2018) High-performance sodium-ion hybrid capacitors based on an interlayer-expanded MoS₂/rGO composite: surpassing the performance of lithium-ion capacitors in a uniform system. *NPG Asia Mater* 10:775–787. <https://doi.org/10.1038/s41427-018-0073-y>
- [8] Zhang W, Liu D, Edwards DD (2016) Self-supported lithium titanium oxide nanosheet arrays decorated with molybdenum disulfide for high-performance lithium-ion batteries. *Energy Technol* 4:1420–1426. <https://doi.org/10.1002/ente.201600187>
- [9] Feng C, Ma J, Li H et al (2009) Synthesis of molybdenum disulfide (MoS₂) for lithium ion battery applications. *Mater Res Bull* 44:1811–1815. <https://doi.org/10.1016/j.materresbull.2009.05.018>
- [10] Shao J, Qu Q, Wan Z et al (2015) From dispersed microspheres to interconnected nanospheres: carbon-sandwiched monolayered MoS₂ as high-performance anode of Li-Ion batteries. *ACS Appl Mater Interfaces* 7:22927–22934. <https://doi.org/10.1021/acsami.5b06002>
- [11] Yu X-Y, Hu H, Wang Y et al (2015) Ultrathin MoS₂ nanosheets supported on n-doped carbon nanoboxes with enhanced lithium storage and electrocatalytic properties. *Angew Chem* 127:7503–7506. <https://doi.org/10.1002/ange.201502117>
- [12] Zhou J, Qin J, Zhang X et al (2015) 2D space-confined synthesis of few-layer MoS₂ anchored on carbon nanosheet for lithium-ion battery anode. *ACS Nano* 9:3837–3848. <https://doi.org/10.1021/nm506850e>
- [13] Stephenson T, Li Z, Olsen B, Mitlin D (2014) Lithium ion battery applications of molybdenum disulfide (MoS₂) nanocomposites. *Energy Environ Sci* 7:209–231. <https://doi.org/10.1039/c3ee42591f>
- [14] Xiao J, Choi D, Cosimbescu L et al (2010) Exfoliated MoS₂ nanocomposite as an anode material for lithium ion batteries. *Chem Mater* 22:4522–4524. <https://doi.org/10.1021/cm101254j>
- [15] Teng Y, Zhao H, Zhang Z et al (2016) MoS₂ nanosheets vertically grown on graphene sheets for lithium-ion battery anodes. *ACS Nano* 10:8526–8535. <https://doi.org/10.1021/acsnano.6b03683>
- [16] Fu W, Li Y, Chensung M et al (2020) An orderly arrangement of layered carbon Nanosheet/TiO₂ nanosheet stack with superior artificially interfacial lithium pseudocapacity. *J Power Sources* 468:228363. <https://doi.org/10.1016/j.jpowsour.2020.228363>
- [17] Ji K, Han J, Hirata A et al (2019) Lithium intercalation into bilayer graphene. *Nat Commun* 10:1–10. <https://doi.org/10.1038/s41467-018-07942-z>
- [18] Ma L, Zhao B, Wang X et al (2018) MoS₂ nanosheets vertically grown on carbonized corn stalks as lithium-ion battery anode. *ACS Appl Mater Interfaces* 10:22067–22073. <https://doi.org/10.1021/acsami.8b04170>
- [19] Sahu TS, Mitra S (2015) Exfoliated MoS₂ sheets and reduced graphene oxide-an excellent and fast anode for sodium-ion battery. *Sci Rep* 5:1–13. <https://doi.org/10.1038/srep12571>
- [20] Ette PM, Chithambararaj A, Prakash AS, Ramesha K (2020) MoS₂ nanoflower-derived interconnected CoMoO₄ nanoarchitectures as a stable and high rate performing anode for lithium-ion battery applications. *ACS Appl Mater Interfaces* 12:11511–11521. <https://doi.org/10.1021/acsami.9b20751>
- [21] Wang J, Zhao X, Fu Y, Wang X (2017) A molybdenum disulfide/reduced oxide-graphene nanoflakelet-on-sheet structure for lithium ion batteries. *Appl Surf Sci* 399:237–244. <https://doi.org/10.1016/j.apsusc.2016.12.029>
- [22] Kong J, Zhao C, Wei Y, Lu X (2015) MoS₂ nanosheets hosted in polydopamine-derived mesoporous carbon nanofibers as lithium-ion battery anodes: enhanced mos2 capacity utilization and underlying mechanism. *ACS Appl Mater Interfaces* 7:24279–24287. <https://doi.org/10.1021/acsami.5b07950>
- [23] Wan L, Sun W, Shen J, Li X (2016) MgO-template-assisted synthesis of worm-like carbon@MoS₂ composite for lithium ion battery anodes. *Electrochim Acta* 211:962–971. <https://doi.org/10.1016/j.electacta.2016.06.115>
- [24] Zhao B, Wang Z, Gao Y et al (2016) Hydrothermal synthesis of layer-controlled MoS₂/graphene composite aerogels for

- lithium-ion battery anode materials. *Appl Surf Sci* 390:209–215. <https://doi.org/10.1016/j.apsusc.2016.08.078>
- [25] Fang Y, Lv Y, Gong F et al (2016) Synthesis of 2D-mesoporous-carbon/MoS₂ heterostructures with well-defined interfaces for high-performance lithium-ion batteries. *Adv Mater* 28:9385–9390. <https://doi.org/10.1002/adma.201602210>
- [26] Wang T, Zhao G, Sun C et al (2017) Graphene-assisted exfoliation of molybdenum disulfide to fabricate 2D heterostructure for enhancing lithium storage. *Adv Mater Interfaces* 4:1–8. <https://doi.org/10.1002/admi.201601187>
- [27] Ren J, Ren RP, Lv YK (2018) A flexible 3D graphene@CNT@MoS₂ hybrid foam anode for high-performance lithium-ion battery. *Chem Eng J* 353:419–424. <https://doi.org/10.1016/j.cej.2018.07.139>
- [28] Zhang C, Jiang Z, Lu B et al (2019) MoS₂ nanoplates assembled on electrospun polyacrylonitrile-metal organic framework-derived carbon fibers for lithium storage. *Nano Energy* 61:104–110. <https://doi.org/10.1016/j.nanoen.2019.04.045>
- [29] Yao SS, He YP, Arslan M et al (2021) The electrochemical behavior of nitrogen-doped carbon nanofibers derived from a polyacrylonitrile precursor in lithium sulfur batteries. *Xinxiang Tan Cailiao/New Carbon Mater* 36:606–615. [https://doi.org/10.1016/S1872-5805\(21\)60032-X](https://doi.org/10.1016/S1872-5805(21)60032-X)
- [30] Hong S, Sheng C, Krishnamoorthy A et al (2018) Chemical vapor deposition synthesis of MoS₂ layers from the direct sulfidation of MoO₃ surfaces using reactive molecular dynamics simulations. *J Phys Chem C* 122:7494–7503. <https://doi.org/10.1021/acs.jpcc.7b12035>
- [31] Nguyen EP, Carey BJ, Daeneke T et al (2015) Investigation of two-solvent grinding-assisted liquid phase exfoliation of layered MoS₂. *Chem Mater* 27:53–59. <https://doi.org/10.1021/cm502915f>
- [32] Liu W, Zhao C, Zhou R et al (2015) Lignin-assisted exfoliation of molybdenum disulfide in aqueous media and its application in lithium ion batteries. *Nanoscale* 7:9919–9926. <https://doi.org/10.1039/c5nr01891a>
- [33] De Moraes ACM, Hyun WJ, Luu NS et al (2020) Phase-inversion polymer composite separators based on hexagonal boron nitride nanosheets for high-temperature lithium-ion batteries. *ACS Appl Mater Interfaces* 12:8107–8114. <https://doi.org/10.1021/acsami.9b18134>
- [34] Liu B, Huang Y, Cao H et al (2018) A novel porous gel polymer electrolyte based on poly(acrylonitrile-polyhedral oligomeric silsesquioxane) with high performances for lithium-ion batteries. *J Memb Sci* 545:140–149. <https://doi.org/10.1016/j.memsci.2017.09.077>
- [35] Lim DH, Manuel J, Ahn JH et al (2012) Polymer electrolytes based on poly(vinylidene fluoride-co-hexafluoropropylene) nanofibrous membranes containing polymer plasticizers for lithium batteries. *Solid State Ionics* 225:631–635. <https://doi.org/10.1016/j.ssi.2012.03.028>
- [36] Han C, Zhang X, Xu X et al (2018) Porous CaFe₂O₄ as a promising lithium ion battery anode: a trade-off between high capacity and long-term stability. *Nanoscale* 10:12963–12969. <https://doi.org/10.1039/c8nr03840f>
- [37] Gao J, He J, Wang N et al (2019) Robust C-S bond integrated graphdiyne-MoS₂ nanohybrids for enhanced lithium storage capability. *Chem Eng J* 373:660–667. <https://doi.org/10.1016/j.cej.2019.05.086>
- [38] Peng H, Wang X, Zhao Y et al (2017) Enhanced electrochemical performance of sulfur/polyacrylonitrile composite by carbon coating for lithium/sulfur batteries. *J Nanoparticle Res.* <https://doi.org/10.1007/s11051-017-4049-6>
- [39] Konarov A, Gosselink D, Doan TNL et al (2014) Simple, scalable, and economical preparation of sulfur-PAN composite cathodes for Li/S batteries. *J Power Sources* 259:183–187. <https://doi.org/10.1016/j.jpowsour.2014.02.078>
- [40] Wei W, Wang J, Zhou L et al (2011) CNT enhanced sulfur composite cathode material for high rate lithium battery. *Electrochem Commun* 13:399–402. <https://doi.org/10.1016/j.elecom.2011.02.001>
- [41] Wang S, Qin C, Feng T et al (2021) Enhanced super capacitive performance of polyacrylonitrile derived hierarchical porous carbon via hybridizing with MoS₂ nanosheets. *J Energy Storage* 40:102695. <https://doi.org/10.1016/j.est.2021.102695>
- [42] McGraw R, Madden WG, Bergren MS et al (1978) A theoretical study of the OH stretching region of the vibrational spectrum of ice Ih. *J Chem Phys* 69:3483–3496. <https://doi.org/10.1063/1.437081>
- [43] Yi M, Zhang C (2018) The synthesis of two-dimensional MoS₂ nanosheets with enhanced tribological properties as oil additives. *RSC Adv* 8:9564–9573. <https://doi.org/10.1039/c7ra12897e>
- [44] Wang J, Liu J, Chao D et al (2014) Self-assembly of honeycomb-like MoS₂ nanoarchitectures anchored into graphene foam for enhanced lithium-ion storage. *Adv Mater* 26:7162–7169. <https://doi.org/10.1002/adma.201402728>
- [45] Seh ZW, Sun Y, Zhang Q, Cui Y (2016) Designing high-energy lithium-sulfur batteries. *Chem Soc Rev* 45:5605–5634. <https://doi.org/10.1039/c5cs00410a>
- [46] Xiong X, Wang Z, Yan G et al (2014) Role of V₂O₅ coating on LiNiO₂-based materials for lithium ion battery. *J Power Sources* 245:183–193. <https://doi.org/10.1016/j.jpowsour.2013.06.133>
- [47] Feng Y, Wu K, Ke J et al (2020) Exfoliated graphite nanosheets wrapping on MoO₂-SnO₂ nanoparticles as a

- high performance anode material for lithium ion batteries. *J Power Sources* 467:228357. <https://doi.org/10.1016/j.jpowsour.2020.228357>
- [48] Zhang Y, Peng Y, Wang Y et al (2017) High sulfur-containing carbon polysulfide polymer as a novel cathode material for lithium-sulfur battery. *Sci Rep* 7:1–9. <https://doi.org/10.1038/s41598-017-11922-6>
- [49] Pender JP, Jha G, Youn DH et al (2020) Electrode degradation in lithium-ion batteries. *ACS Nano* 14:1243–1295. <https://doi.org/10.1021/acsnano.9b04365>
- [50] Cao M, Gao L, Lv X, Shen Y (2017) $\text{TiO}_2\text{-B@VS}_2$ heterogeneous nanowire arrays as superior anodes for lithium-ion batteries. *J Power Sources* 350:87–93. <https://doi.org/10.1016/j.jpowsour.2017.03.070>

Publisher's Note Springer Nature remains neutral with regard to jurisdictional claims in published maps and institutional affiliations.